

The freshwater balance of polar regions in transient simulations from 1500 to 2100 AD using a comprehensive coupled climate model

Flavio Lehner · Christoph C. Raible ·
Dominik Hofer · Thomas F. Stocker

Received: 4 March 2011 / Accepted: 14 September 2011 / Published online: 5 October 2011
© The Author(s) 2011. This article is published with open access at Springerlink.com

Abstract The ocean and sea ice in both polar regions are important reservoirs of freshwater within the climate system. While the response of these reservoirs to future climate change has been studied intensively, the sensitivity of the polar freshwater balance to natural forcing variations during preindustrial times has received less attention. Using an ensemble of transient simulations from 1500 to 2100 AD we put present-day and future states of the polar freshwater balance in the context of low frequency variability of the past five centuries. This is done by focusing on different multi-decadal periods of characteristic external forcing. In the Arctic, freshwater is shifted from the ocean to sea ice during the Maunder Minimum while the total amount of freshwater within the Arctic domain remains unchanged. In contrast, the subsequent Dalton Minimum does not leave an imprint on the slow-reacting reservoirs of the ocean and sea ice, but triggers a drop in the import of freshwater through the atmosphere. During the twentieth and twenty-first century the build-up of freshwater in the Arctic Ocean leads to a strengthening of the liquid export. The Arctic freshwater balance is shifted towards being a large source of freshwater to the North Atlantic ocean. The Antarctic freshwater cycle, on the other hand, appears to be insensitive to preindustrial variations in external forcing. In line with the rising temperature during the industrial era the freshwater budget becomes increasingly unbalanced and strengthens the high latitude's Southern Ocean as a source of liquid freshwater to lower latitude oceans.

Keywords Freshwater balance · Hydrological cycle · Polar climate · Little Ice Age · External forcing

1 Introduction

The hydrological cycle is of crucial importance for the climate system in terms of energy, moisture, and nutrient distribution (Allen and Ingram 2002). Socio-economic impacts of climate and climate change are often closely linked to the corresponding regional characteristics of the hydrological cycle (floods, droughts; IPCC 2007). Along with a broad consensus on the recent and projected future anthropogenic global warming, an intensification of the hydrological cycle is expected based on the Clausius-Clapeyron relation which suggests specific humidity to increase exponentially with temperature (approximately $7\% K^{-1}$; IPCC 2007). In fact, widespread evidence for such an intensification is already available from twentieth century observations, as summarized, e.g., in Huntington (2005), White et al. (2007), and Syed et al. (2010).

Additionally, numerous model studies are able to reproduce the intensification of the hydrological cycle in the second half of the twentieth century and project it to continue in the twenty-first century (Wu et al. 2005; Held and Soden 2006; IPCC 2007; Williams et al. 2007; Khon et al. 2010; Seager et al. 2010). Wu et al. (2005) found the freshwater forcing to the ocean surface to change in a non-uniform way across latitudes. While high latitudes tend to receive more freshwater, the sub-tropics will receive less. However, as the rate of change of the freshwater forcing in the northern high latitudes is larger than in the southern high latitudes the question about a possible global redistribution of major water masses in the hydrological cycle and specifically in the ocean arises (Stocker and Raible 2005; Peterson et al. 2006).

F. Lehner (✉) · C. C. Raible · D. Hofer · T. F. Stocker
Climate and Environmental Physics, Physics Institute,
and Oeschger Centre for Climate Change Research,
University of Bern, Sidlerstrasse 5, 3012 Bern, Switzerland
e-mail: lehner@climate.unibe.ch

One example of major water masses are the large quantities of freshwater stored in liquid and solid form in both polar regions. This freshwater, once released, can alter the hydrography and circulation in ocean basins (Peterson et al. 2002). The cycling of freshwater within polar regions, as well as the exchange with sub-polar latitudes, is driven by an interplay of oceanic and atmospheric quantities and processes, of which many are known to respond to interannual to decadal variations in temperature, e.g., atmospheric moisture content, atmospheric circulation, sea ice extent, volume, and transport. Such variations in temperature can be caused by anthropogenic greenhouse gases (GHGs) or natural forcing, such as volcanic eruptions or changes of the solar irradiance.

The purpose of this study is to put results from climate model simulations of present-day and future polar climate in the context of multi-decadal variability of the past five centuries. We focus on the freshwater cycling within the polar regions as well as the meridional exchange with lower latitudes. The study complements earlier work which address the hydrological cycle in polar regions with a focus on the industrial era and on the Arctic Ocean alone (Holland et al. 2006b; Koenigk et al. 2007; Arzel et al. 2008).

To investigate the freshwater cycle in the polar regions at different climate states, and to estimate its sensitivity to natural and anthropogenic forcing, we analyze simulations with a coupled General Circulation Model (GCM), applying transient external forcing from 1500 to 2100 AD.

This paper is structured as follows: a description of the model and experimental setup as well as a short validation of the simulations are presented in Sect. 2. In Sects. 3 and 4 we examine the simulated freshwater budgets of both polar regions, subdivided in (1) present-day state, (2) changes in the preindustrial era, and (3) future projections. A summary and conclusions follow in Sect. 5.

2 Model and methods

2.1 Model

The model used for the simulations is the Community Climate System Model version 3.0.1 (CCSM3), which was developed by the National Center for Atmospheric Research (NCAR) (Collins et al. 2006). The model includes four components, namely the atmosphere, ocean, sea ice, and land surface, all linked through a coupler which exchanges fluxes (without flux corrections) and state information. We selected the low-resolution version: 3.75° by 3.75° in the atmosphere (26 vertical levels) and on land and a sea ice and ocean resolution of about 3.6° in longitude and 0.6° to 2.8° in latitude with finer resolution in the tropics and around Greenland, allowing for an open

passage through the Canadian Arctic Archipelago. The ocean has 25 levels and a rigid lid. The land model does not include a dynamic ice sheet model but is able to lose and grow snow and ice up to $1,000 \text{ kg m}^{-2}$. Additional mass above this threshold is inserted into runoff. We discuss the implications of a missing ice sheet model for our study in Sect. 5.

More detailed descriptions of the model components are available at the NCAR CCSM webpage (<http://www.cesm.ucar.edu/models/ccsm3.0>). The version used here and its simulation of present-day climate is comprehensively described in Yeager et al. (2006).

2.2 Experimental setup

For this and other studies (Yoshimori et al. 2010; Hofer et al. 2011) a series of model simulations was conducted. In this paper we use the following two setups: a 1500 AD equilibrium simulation with perpetual 1500 AD conditions (hereafter CTRL1500) and an ensemble of four transient simulations from 1500 to 2100 AD (TRa1 to TRa4, as in Hofer et al. 2011).

The transient simulations were branched from different years of the multi-century control simulation CTRL1500. The CTRL1500 simulation itself was initialized from a control simulation with perpetual 1990 AD conditions, an extension of the simulation presented by Yeager et al. (2006). As the CTRL1500 simulation has not fully reached an equilibrium state it exhibits a slight drift. Therefore, all transient simulations branched from the CTRL1500 inherit this drift as well and need to be corrected for it by detrending them with a quadratic fit estimated from CTRL1500 for every quantity, grid point, and month. For most quantities the trends are in the order of $0.01\text{--}0.02\% \text{ year}^{-1}$. The time-varying forcing consists of GHG concentrations, solar forcing, and volcanic aerosols and is summarized in Fig. 1. For details on the detrending technique and on the forcing datasets the reader is referred to Hofer et al. (2011).

Our analysis focuses on six 31-year periods with different forcing levels: the quasi-equilibrium period just after branching from CTRL1500 which corresponds approximately to the beginning of the Little Ice Age (Mann et al. 2009), when the solar forcing generally is lower than today (averaged over 1500–1530 AD, hereafter Initial Conditions); the period of the pronounced solar forcing minimum of the Maunder Minimum (1685–1715 AD); the Dalton Minimum (1800–1830 AD), when a solar forcing minimum coincides with two large eruptions of tropical volcanoes; a period when GHGs start to increase (1840–1870 AD, Pre-industrial); a period of present-day climate (1960–1990 AD, Present-Day) and finally, a period at the end of the twenty-first century when the average radiative forcing is projected to be approximately 5 W m^{-2} larger than 1990

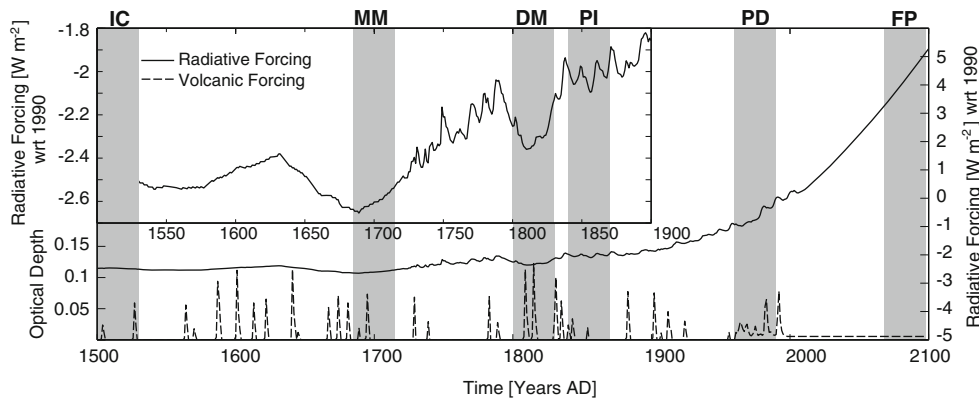


Fig. 1 Natural and anthropogenic forcing used in the simulations: the combined radiative forcing from GHGs and solar irradiance in W m^{-2} , calculated as in IPCC (2001) with reference to (wrt) 1990 (solid line), assuming a global average albedo of 0.3, and the volcanic forcing as optical depth (dashed). The inset highlights the changes in forcing by stretching the vertical scale, however, the curve is the same as in the main

AD (2068–2098 AD, Future Projections). For the twenty-first century we apply the IPCC SRES A2 scenario (IPCC SRES 2000).

2.3 Methods

Freshwater budgets and transports are computed from the monthly means of the four ensemble members, however, in figures and tables we show annual means. The spatial domains are $60\text{--}90^\circ\text{N}$ (as in ACIA (2005)) and $60\text{--}90^\circ\text{S}$. This selection enables us to compare equivalent areas at both polar regions and to include all major processes influencing the polar freshwater balance. To compute the freshwater balance we need to consider the atmospheric import of water, i.e., meridional water transport VQ (including eddy-induced transport), precipitation P , and evaporation E over land ($_{lnd}$), ocean ($_{ocn}$), and sea ice ($_{ice}$). Water imported into the domain over land by rivers that cross the 60°N boundary from the south as well as the discharge into the oceans (called R) is calculated by the river transport model. This is a 2-dimensional model on an independent 0.5° by 0.5° grid. The land model also allows for a limited storage of water and ice in grid cells defined as wetland and glaciers, thus changes in soil moisture, glacier mass, and permafrost are crudely represented in the model. The sea ice and ocean budget terms include the storage and transport of freshwater. The ocean liquid freshwater (FW) storage is computed as

$$FW(S) = \int \int_{z_{max}}^{z_1} \frac{S_0 - S}{S_0} dz dA, \quad (1)$$

with S being the in-situ salinity and S_0 a reference salinity. z covers all model levels while A represents the ocean

plot. Further details on the forcing dataset can be found in Hofer et al. (2011). The time periods as used throughout the study are indicated by the vertical bars and labeled at the top: Initial Conditions (IC, 1500–1530 AD), Maunder Minimum (MM, 1685–1715 AD), Dalton Minimum (DM, 1800–1830 AD), Preindustrial (PI, 1840–1870 AD), Present-Day (PD, 1960–1990 AD), and Future Projections (FP, 2068–2098 AD)

domain’s area. The ocean freshwater transport across a transect is

$$FWT(u, S) = \int_{l_1}^{l_2} \int_{z_{max}}^{z_1} u \frac{(S_0 - S)}{S_0} dz dl, \quad (2)$$

where u is the horizontal velocity perpendicular to the transect and l_1 and l_2 are the start and end point of the transect, defining its length.

In Eqs. (1) and (2) S_0 is estimated from the CTRL1500 so that the complete freshwater budget for the Arctic domain is closed in its initial state under perpetual 1500 AD conditions. This means that total net import of freshwater into the Arctic domain is nearly zero at year 1500 AD. This leads to a S_0 of 34.88 g kg^{-1} for the Arctic domain. In the Antarctic domain, however, using monthly instead of instantaneous values to calculate the FW transport introduces significant errors as the meridional velocity field shows strong variations on sub-monthly time scales. To overcome this problem we use a different approach to estimate the FW transport for the Antarctic domain, i.e., the residual from changes in FW storage (with $S_0 = 34.88 \text{ g kg}^{-1}$) and all ocean surface freshwater fluxes:

$$FWT(t) = FW(t+1) - FW(t) - \frac{P_{ocn}(t) + P_{ocn}(t+1)}{2} - \frac{E_{ocn}(t) + E_{ocn}(t+1)}{2} + \frac{R(t) + R(t+1)}{2} + \frac{M(t) + M(t+1)}{2} \quad (3)$$

where M is the melt flux from sea ice and t indexing the monthly time-stepping. A comprehensive description of the significance of the reference salinity can be found in Serreze et al. (2006), and with respect to rigid lid ocean

model components in Pardaens et al. (2003). For the sea ice storage and transport, where the error from using monthly means is negligible, the salinity is set to 4 g kg^{-1} in the model. Finally, freshwater exchange rates between sea ice and ocean are calculated, whereby precipitation that directly runs off the sea ice into the ocean is included in the flux from the sea ice to the ocean.

2.4 Validation

The CCSM3 has been thoroughly tested for various resolutions (Hack et al. 2005; Yeager et al. 2006; Kiehl et al. 2006; Bryan et al. 2006; Holland et al. 2006a, b). Generally, the low-resolution version differs more strongly from observations than the middle or high-resolution version. This is largely due to the fact that the middle and high-resolution versions both run with the higher resolved 1° ocean/sea ice component. This has implications for properties such as salinity, heat flux, sea ice extent and volume as will be discussed here.

The simulated annual mean surface air temperature (SAT) evolution on the Northern Hemisphere (NH) over the past five centuries is in good agreement with reconstructions, except for an overestimation of the twentieth century warming due to the absence of sulfate aerosols in the simulations (Hofer et al. 2011). The twenty-first century is dominated by the rapid increase in GHGs (as prescribed by the IPCC SRES A2 scenario), which results in an ensemble mean NH warming of 2.9°C , calculated as the difference between the averages over the periods 1990–2000 AD and 2088–2098. The equilibrium climate sensitivity of the low-resolution version is 2.32°C (Kiehl et al. 2006) and is therefore at the lower end of the range of likely climate sensitivities ($2\text{--}4.5^\circ\text{C}$, IPCC (2007)). The Arctic domain's SAT anomaly ($60\text{--}90^\circ\text{N}$) follows the SAT of the NH including a cooling during the Maunder Minimum and Dalton Minimum (Fig. 2). However, due to the effect of polar amplification (Holland and Bitz 2003; Masson-Delmotte et al. 2006; Bekryaev et al. 2010) the amplitudes are generally about 100% larger than in the hemispheric average. In the Antarctic domain ($60\text{--}90^\circ\text{S}$) on the other hand, no robust signal of the Little Ice Age is detectable (Fig. 2). During the twentieth century, simulations show a smaller trend of Antarctic's domain temperature and variability compared with reanalysis data. Due to the absence of time-variable ozone in the simulations the temperature over Antarctica also does not show the observed late-twentieth century dipole temperature anomaly pattern (as in Thompson and Solomon 2002, not shown). The simulated twenty-first century warming remains below the warming simulated in the Arctic domain due to the comparably weaker sea ice-albedo feedback (Masson-Delmotte et al. 2006; Walsh 2009) and larger

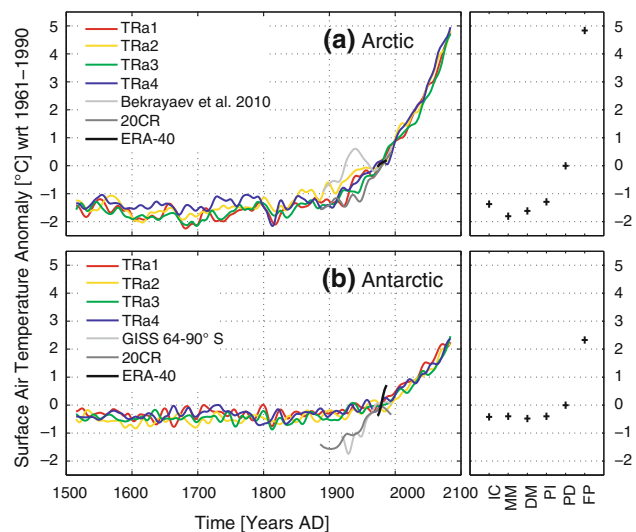
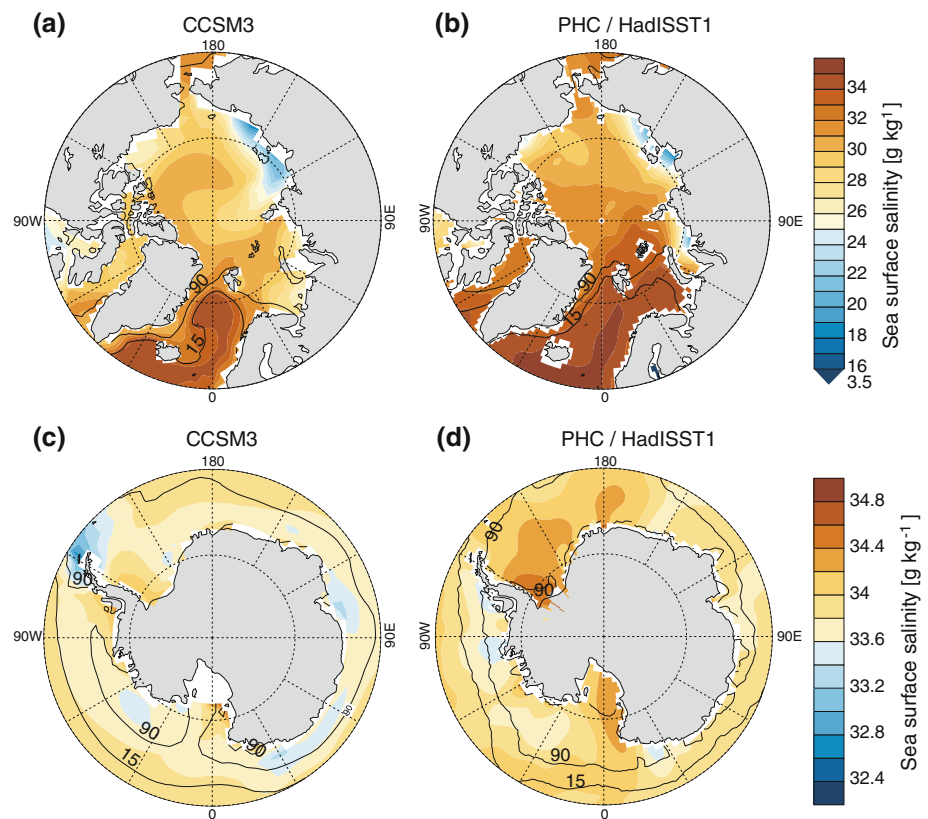


Fig. 2 a Arctic and b Antarctic domain's surface air temperature anomaly with reference to (wrt) 1961–1990 AD. The small panels on the right show mean anomalies for the different time periods Initial Conditions (IC, 1500–1530 AD), Maunder Minimum (MM, 1685–1715 AD), Dalton Minimum (DM, 1800–1830 AD), Preindustrial (PI, 1840–1870 AD), Present-Day (PD, 1960–1990 AD), and Future Projections (FP, 2068–2098 AD). The time series are smoothed by a 30-year Gaussian-weighted filter. Bekryaev et al. (2010) updated the GISS dataset (Hansen et al. 2010) in the Arctic region. 20CR is Compo et al. (2010). ERA-40 data is available from ECMWF in $2.5^\circ \times 2.5^\circ$ resolution

ocean heat uptake. The simulated Arctic domain's ensemble mean during 1980–2000 AD is too cold with a bias of $3.5\text{--}7.3 \text{ K}$, depending on the reanalysis, while the Antarctic domain is too cold by $1.5\text{--}4.1 \text{ K}$. Note that this is within a 10% range of the documented general cold bias of the model (Yeager et al. 2006).

The simulated polar oceans are generally too fresh compared to the salinity field of the Polar Science Center Hydrographic Climatology (PHC, Steele et al. 2001; Fig. 3). In the Arctic Ocean the model is able to reproduce the fresh shelf conditions arising from the shallow water and the river runoff into those, although the detailed spatial pattern is not captured very well. Further, the Beaufort Gyre is larger and stores more freshwater than is estimated from observations (Fig. 4b, compare with Fig. 3 in Serreze et al. 2006). In the Barents Sea, Greenland-Iceland-Norwegian (GIN) Seas, Labrador Sea, Baffin Bay and off the south-eastern coast of Greenland, the model tends to be too fresh. The salinity biases in the Barents Sea are mainly caused by an underestimation of the meridional transport of warm and salty Atlantic waters into the Barents Sea and the Arctic Ocean (Yeager et al. 2006). Along with this the sea ice extends further to the south (especially in the Barents Sea, Fig. 3), which results in a spatial anomalous melt flux. Additionally, the simulated sea ice covers larger areas, suppressing evaporation from the ocean surface and therefore further freshening the ocean.

Fig. 3 Sea surface salinity in the **a, b** Arctic and **c, d** Antarctic domain, from the **b, d** Polar Science Center Hydrographic Climatology (PHC, Steele et al. 2001) and **a, c** model output averaged from 1990 to 1999 AD (*left*). Note the different *color scales* for the Arctic and Antarctic plots. The minimum value of 3.5 g kg^{-1} in the Arctic color scale occurs in the Baltic Sea observations. Contours are 15 and 90% sea ice concentration of March (Arctic) and September (Antarctic) from HadISST1 (Rayner et al. 2003) and the 1990–1999 AD model average. The model land mask is given in *white*



In the Antarctic region the model generally tends to be too fresh as well (Fig. 3). Still, it is able to simulate the more saline areas of the Weddell Sea and Ross Sea but it underestimates the amplitude and spatial extent. Furthermore, the model produces a patch of relatively fresh water at the northern end of the Antarctic Peninsula which is not observed in reality. The pattern of the sea ice concentration around Antarctica generally agrees with observations, while the total sea ice extent and area are overestimated by about 23 and 22%, respectively, during 1990–1999 AD (not shown). Regionally, the sea ice is overestimated in the Atlantic sector and underestimated in the Ross Sea sector.

In recent years efforts in data collection resulted in new estimates of the large-scale Arctic freshwater cycle (Serreze et al. 2006) which is compared to the ensemble mean of this study (Table 1). The numbers from a multi-model study by Holland et al. (2007) are listed for additional comparison. The simulated freshwater budget of the Arctic Ocean is in reasonably good agreement with observations regarding the oceanic and terrestrial freshwater fluxes (FW transport, sea ice transport, R) while the atmospheric fluxes P and E are underestimated by about 30 and 50%, respectively. However, a recent study reveals large uncertainties regarding absolute values still inherent in observations of $P-E$ in the Arctic (Rawlins et al. 2010). The ocean imbalance of our simulations ($194 \pm 331 \text{ km}^3 \text{ year}^{-1}$) is indistinguishable from zero relative to the standard deviation and in this respect

qualitatively agrees with observations, where the imbalance is indistinguishable from zero relative to measurement errors (Serreze et al. 2006). The freshwater reservoir of the ocean is substantially overestimated due to an Arctic Ocean that is too fresh throughout the column with a larger bias in the top 400 m (Fig. 4a). This stands in contrast to the negative freshwater reservoir obtained from the high-resolution CCSM3 of the model set analyzed by Holland et al. (2007). The storage in sea ice is too large as well, a consequence of the too cold Arctic in the low-resolution version. However, the spread among models regarding these two reservoirs is known to be large (Holland et al. 2007). Confidence in the simulated Arctic hydrological cycle arises from the relatively small bias in the transport terms and in the overall balanced budget in the present-day state. For reasons of data lack we refrain from a validation of the Antarctic domain's freshwater budget.

3 Freshwater balance of the Arctic domain

3.1 Present-day climate

The simulated freshwater cycle of the Arctic domain is illustrated in Fig. 5, where the ensemble means for the time periods Initial Conditions, Maunder Minimum, Present-Day and Future Projections are presented. The standard

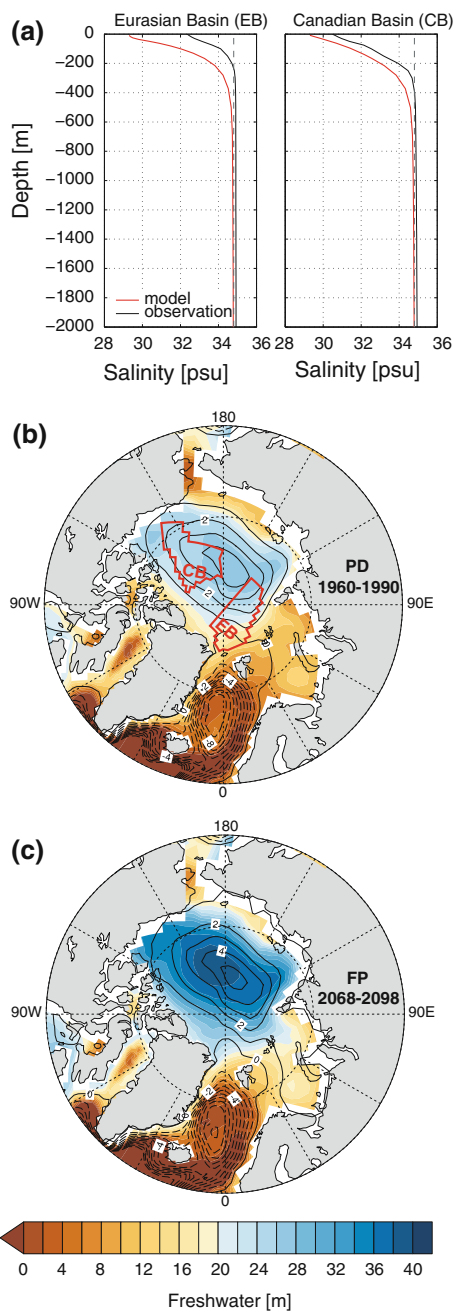


Fig. 4 Salinity profiles, freshwater storage, and barotropic stream function in the Arctic domain. **a** Salinity profiles from the Eurasian (EB) and the Canadian Basin (CB), where the ocean is deeper than 2,000 m from the model (1990–1999 AD ensemble mean) and observations (PHC, Steele et al. 2001). The vertical dashed line marks the reference salinity of 34.8 g kg^{-1} used by Serreze et al. (2006), Holland et al. (2007), and here in **b** and **c**, as well as in Table 1. The basins are indicated in **b** with EB and CB. **b**, **c** FW storage and barotropic stream function for **b** Present-Day (PD, 1960–1999 AD) and **c** Future Projections (FP, 2068–2098 AD). The model land mask is given in white

deviation (\pm) for a specific budget term and time period is estimated from the 124 annual means of the four ensemble members (4×31 years). The difference in mean from

Initial Conditions, the Maunder Minimum and Future Projections to Present-Day is tested for significance for each ensemble member, using a Mann-Whitney rank sum test at the 5% level. A pie chart illustrates the number of ensemble members that show a significant difference between Present-Day and the other time periods (Figs. 5 and 6). This serves as a simple metric for the robustness of a given signal. The same procedure is then used to illustrate changes during the preindustrial era (Table 2). Additionally, time series and running 50-year linear trends of selected budget quantities are presented.

The simulated present-day freshwater cycle of the Arctic domain correctly reflects observations in a qualitative manner. VQ accounts for approximately 91% of the domains' net freshwater import. In agreement with Sorteberg and Walsh (2008) the majority of this import takes place over the Bering Sea and the Eastern North Atlantic/European sector (Fig. 7). The equivalent of less than 3% of this imported freshwater is temporarily stored in the atmosphere as water vapor Q . While land and ocean each cover about 50% of the total domain area, the atmospheric freshwater is preferentially delivered to the land surface where approximately 55% of total P and 65% of total $P-E$ end up. For the ocean the largest net source by far is R (82%), as $P-E$, as well as the freshwater exchange between sea ice and ocean, are each nearly in balance on basis of the annual means. Note that, when focusing on the Arctic Ocean only, this distribution is somewhat different: $P_{ocn} - E_{ocn}$ is positive and the sea ice balance negative (not shown, but in agreement with Serreze et al. (2006)).

We mentioned the overestimated freshwater storage in the ocean and sea ice. The domain's freshwater budget is balanced in part by export of sea ice and ocean freshwater. Thereby, the Labrador and Irminger Sea, and to a smaller extent the western Bering Sea, are the major areas of export for both sea ice and ocean freshwater (Fig. 7). The eastern part of the Bering Sea including the Bering Strait imports about as much ocean freshwater as is exported through the Irminger Sea, thereby providing the second largest source of freshwater to the Arctic domain. Finally, rivers crossing 60°N (e.g., Ob, Yenisey, Lena, see Fig. 7) close the land budget.

3.2 Preindustrial changes

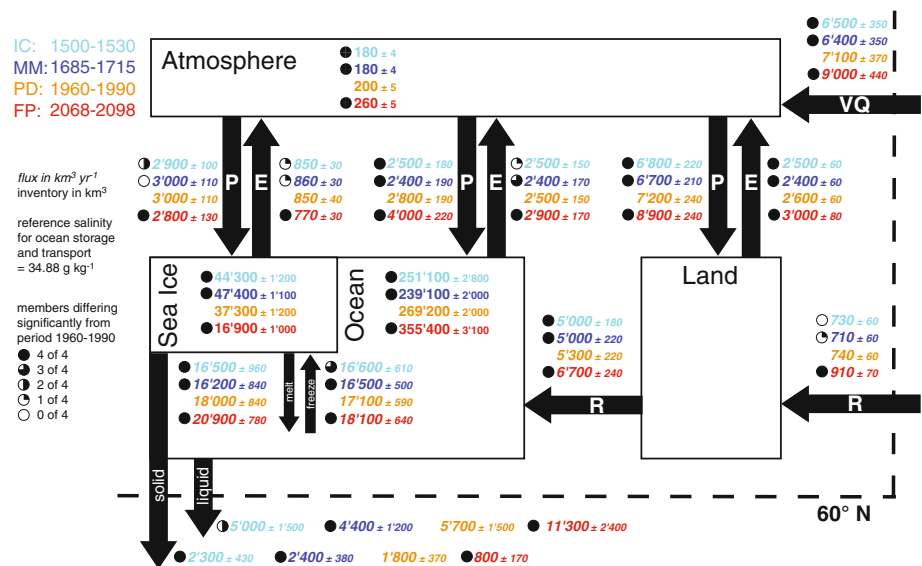
The present-day freshwater budget differs significantly from those during the two preindustrial time periods (Initial Conditions and Maunder Minimum) when NH as well as Arctic temperatures were lower than during Present-Day (see Fig. 2). VQ and Q are significantly smaller during Initial Conditions and the Maunder Minimum, resulting in a decrease of P_{Ind} , P_{ocn} and P_{ice} , i.e., total P over the domain. As a consequence of the reduction in P_{Ind} , R is

Table 1 Ensemble mean freshwater budget of the Arctic Ocean

Study Averaging period	Serreze et al. (2006) ~ 1980–2000 AD	Holland et al. (2007) 1980–1999 AD	This study 1980–2000 AD
Precipitation	3,300 ± 680	2,411 ± 360	2,265 ± 109
Evaporation	−1,300 ± 710	−868 ± 275	−687 ± 32
Runoff	3,200 ± 110	3,162 ± 776	3,482 ± 187
Ocean transp. liquid	−3,450 ± 693		−2,899 ± 569
– without CAA	−250 ± 615	−1,388 ± 2,332	−395 ± 579
Ocean transp. solid	−2,460 ± 340		−1,967 ± 421
– without CAA	−2,300 ± 340	−1,841 ± 626	−1,967 ± 421
Imbalance ocean	−710 ± 1,255		194 ± 331
Storage ocean	24,200	47,756	177,930 ± 1,652
Sea ice storage	10,000	13,851	29,347 ± 2,557

Fluxes in km³ year^{−1}, stores in km³, as calculated in Holland et al. (2007) and with the same reference salinity of 34.8 g kg^{−1}. Fluxes leaving the Arctic Ocean are negative. ± Corresponds to the measurement error and to the measurement error propagation in case of the ocean imbalance for Serreze et al. (2006); to the inter-model standard deviation for Holland et al. (2007); and to the standard deviation of the four ensemble members for this study. Holland et al. (2007) provide no numbers for the transport through the Canadian Arctic Archipelago (CAA) because most models investigated did not have an open passage through the CAA

Fig. 5 Freshwater budget of 60–90°N. Values are ensemble mean 31-year averages according to the color shading in the upper left corner: Initial Conditions (IC), Maunder Minimum (MM), Present-Day (PD), and Future Projections (FP). Further details in the text



reduced as well. Changes in E during Initial Conditions and the Maunder Minimum are robust only over land where E_{lna} is significantly decreased. The sea ice volume is significantly larger in Initial Conditions and the Maunder Minimum than during Present-Day, resembling the colder conditions of the preindustrial era.

The sea ice volume maximum is reached during the Maunder Minimum when the annual sea ice growth exceeds the melt rate by approximately 300 km³ year^{−1}. Not surprisingly, the sea ice export reaches a maximum as well during that time. The ocean liquid freshwater export (FW transport), on the other hand, is significantly reduced during Initial Conditions and the Maunder Minimum. However, the ocean as a whole is saltier, i.e., stores less freshwater than

during Present-Day. This is largely because during the Maunder Minimum sea ice grows, resulting in a negative freshwater flux to the ocean surface. In other words, brine rejection from the sea ice growth makes the ocean saltier and overcompensates for the reduced FW transport. In fact, the sum of all fluxes to and from the ocean (through the surface and ocean-internal) during the Maunder Minimum is less than half of that during Present-Day (300 vs. 800 km³ year^{−1}). Due to large internal variability, however, this difference is significant only in two ensemble members.

The detection of significant and robust changes within the preindustrial era (Initial Conditions-Preindustrial, 1500–1870 AD) proves to be difficult as the interannual variability of several budget terms is high; although in

Fig. 6 As Fig. 5, but for 60–90°S

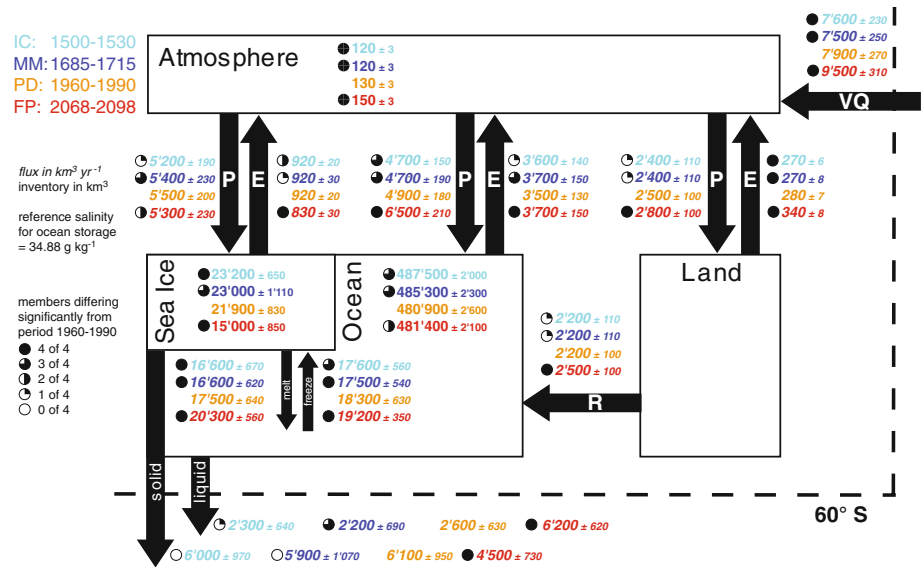


Table 2 Domain freshwater storage and transport terms at the boundary

Domain	Budget term	MM–IC	DM–IC	DM–MM	PI–IC	PI–MM	PI–DM
60–90° N	FW storage (ocean storage)	●*	●	●	●	●	●
	Sea ice storage	●	●	●	●	●	●
	Q (atmosphere storage)	●	●	●	●	●	●
	FW transport (ocean export)	●	○	○	○	○	○
	Sea ice export	●	○	○	○	○	○
	VQ (atmosphere import)	○	○	○	●	●	●
60–90° S	FW storage	●	●	○	●	●	●
	Sea ice storage	●	○	○	●	●	●
	Q	○	○	○	○	○	○
	FW transport	○	○	○	○	○	○
	Sea ice export	○	○	○	○	○	○
	VQ	●	●	○	○	○	○

* members with significant difference, e.g.:

● 4 of 4 ● 3 of 4 ● 2 of 4 ● 1 of 4 ○ 0 of 4

● 2 members increase, 1 member decrease, 1 insignificant

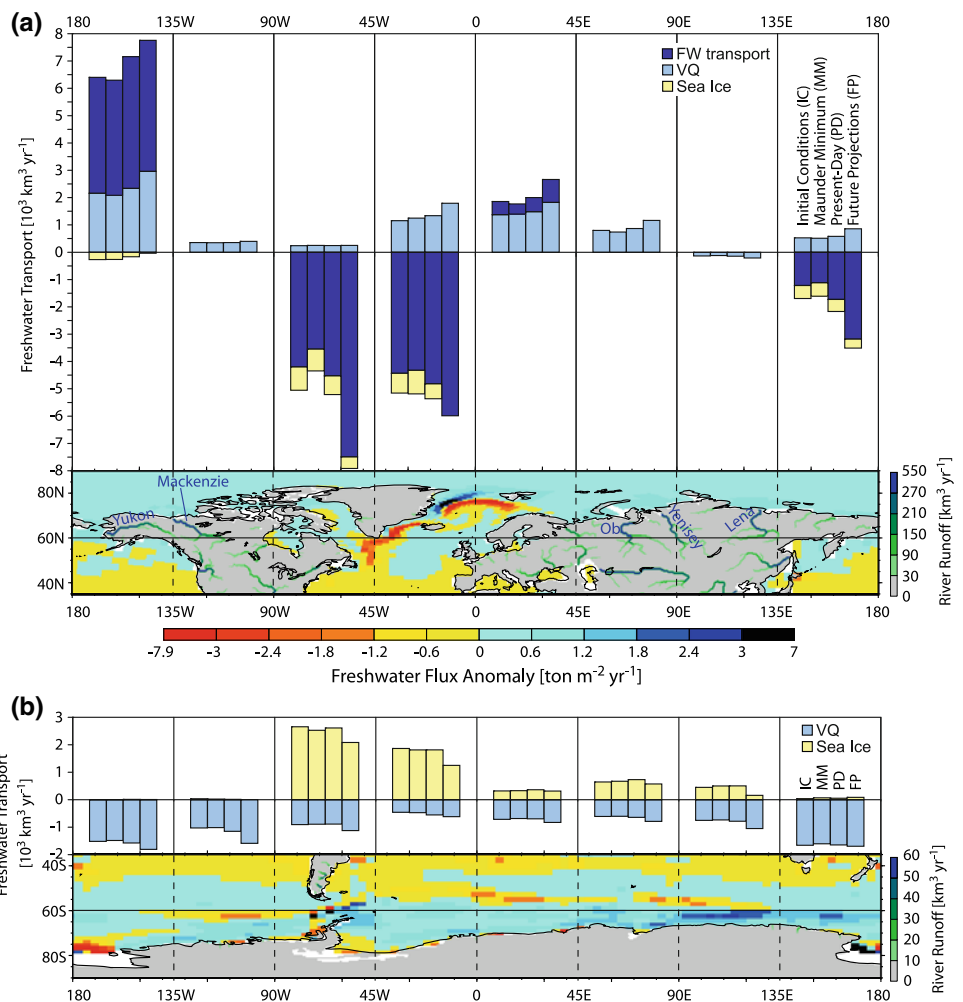
Number of ensemble members, which show a significant change between certain preindustrial time periods, is given as pie chart. *Black* denotes an positive difference in mean between two time periods, *gray* a negative difference. This gives a hint whether the sign of a trend is consistent among ensemble members and how robust that trend is. *Time periods*: Initial Conditions (IC, 1500–1530 AD), Maunder Minimum (MM, 1685–1715 AD), Dalton Minimum (DM, 1800–1830 AD), and Preindustrial (PI, 1840–1870 AD)

observations of the Arctic freshwater cycle interannual variability is even larger than in GCMs (Rawlins et al. 2010). Prior to Preindustrial the freshwater balance of the Arctic domain as a whole is stable with the only notable change being internal redistribution of freshwater masses. Table 2 compares selected quantities of the polar freshwater budgets for different preindustrial time periods: FW storage, sea ice storage, and Q are storage terms inside the domain, while FW transport, sea ice export and VQ are transport terms at the domain’s boundary. With the comparison of Initial Conditions, the Maunder Minimum, and

the Dalton Minimum we try to determine whether these three periods of similarly weak external forcing differ significantly among each other.

In general, changes between Initial Conditions and the Maunder Minimum are more robust in the storage terms than in the transport terms. This can be seen by the significant reduction of FW storage in all and of Q in three of the ensemble members, respectively. In concert with that, the sea ice storage significantly increases in three members. This is consistent with the absolute numbers in Fig. 5 where sea ice grows at the expense of FW, while all

Fig. 7 Ensemble mean freshwater transport as *liquid* (*FW* transport), water vapor (*VQ*), and *solid* (sea ice) across 60°N (a) and 60°S (b), summed up over 45° longitudinal transects; *positive values* indicate a northward transport. The *bars* in the chart correspond to the time periods Initial Conditions (IC, 1500–1530 AD), Maunder Minimum (MM, 1685–1715 AD), Present-Day (PD, 1960–1990 AD), and Future Projections (FP, 2068–2098 AD). Due to the computation of *FW* transport from residuals on the SH it is not possible to show this term for each sector. The *bottom panels* in **a** and **b** show the ensemble mean freshwater flux ($P - E + R +$ sea ice melt flux) anomaly of FP minus PD, as well as river runoff during PD. The model land mask is given in *white*



transport terms at the domain’s boundary change only insignificantly. Comparing Initial Conditions to the Dalton Minimum, the decrease in *FW* storage is the only significant and robust change. Comparing the Maunder Minimum to the Dalton Minimum, the reduction of the sea ice storage is the only robust change. All other changes are either not significant or, if they are, do not show a consistent sign of change among the ensemble members. This allows for a first conclusion that the difference between the three periods Initial Conditions, Maunder Minimum and Dalton Minimum is characterized by minor redistributions of freshwater between the reservoirs of the ocean and sea ice. At the same time, the total amount of freshwater in the domain does not change notably.

To relate these domain-internal redistributions of the freshwater to changes in the external forcing, we show the transient behavior of the different budget terms (Fig. 8). The exact timing of change in the Arctic *FW* storage is not linearly connected to the external forcing. This manifests itself in the coexistence of positive and negative trends in

the *FW* storage ensemble members and the following substantial spread among the members during the seventeenth and eighteenth century (Fig. 8a). Note that the members originally started from only slightly different initial conditions and have experienced identical external forcing since. Thus to a large extent the decadal changes in *FW* storage in the preindustrial era are driven by internal variability. In fact, for the ensemble members TRa2 and TRa3 the timing of the transition of *FW* storage from its initial conditions to a lower value coincides with similar transitions found in time series of Atlantic maximum overturning circulation (AMOC) from the same simulations (Hofer et al. (2011); using their method to determine the transition phase). In these cases, a weaker AMOC is largely responsible for a decrease in salinity in the GIN Seas and the Atlantic part of the Arctic domain. The salinity decrease in these areas in turn is crucial to explain the decrease of the Arctic domains’s total *FW* storage during that time. However, this indirect attribution of ramp-like *FW* storage changes to variations in the AMOC

is not robust throughout the ensemble—but a further investigation is beyond the scope of this study. The running trend of the sea ice storage, opposed to one of *FW* storage, follows the variations in external forcing more closely (Fig. 8b).

The atmospheric terms Q , VQ , total $P-E$, and R (which is largely controlled by $P_{Ind}-E_{Ind}$) do not show a significant response in the Maunder Minimum, but gradually increase along with the radiative forcing from the Maunder Minimum onwards (Fig. 8c, e, f). During the Dalton Minimum, however, these terms experience an abrupt dip. This dip sets them back to values similar as during Initial Conditions and the Maunder Minimum, even though the radiative forcing from solar and GHGs was approximately 5 and 10% weaker during Initial Conditions and the Maunder Minimum than during the Dalton Minimum, respectively. This raises the question of the necessity of the volcanic forcing to explain the atmospheric state of the Arctic freshwater balance during the Dalton Minimum. On a shorter time scale, the atmospheric response to volcanoes has been investigated using a composite of the years following the 21 largest eruptions from 1500 to 2000 AD (not shown). There, no significant large-scale response on high latitude total $P-E$ and VQ could be detected. However, $P-E$ and VQ are reduced just at 60°N in the first 2 years after an eruption. This contributes to the simulated reduction in the fields of $P-E$ and VQ during the Dalton Minimum, nevertheless, the solar forcing is the main driver. Note that while the direct radiative effects from volcanic aerosols are correctly represented in the CCSM3, it has its deficits in simulating the dynamical effects of volcanic eruptions. This is namely the absence of the NH mid- to high-latitude winter-warming pattern that would result from a positive phase of the North Atlantic Oscillation (Stenchikov et al. 2006). Interestingly, Schneider et al. (2009) found a winter-warming in idealized experiments with the medium resolution version of CCSM3 while the high (Stenchikov et al. 2006) and low-resolution version do not reproduce this pattern.

As the solar minimum of the Dalton Minimum ceases and GHGs start to increase the combined radiative forcing exceeds the preceding range since 1500 AD and so does the Arctic domain's SAT (Fig. 2). As a consequence the atmospheric terms VQ , Q , and total $P-E$ recover to pre-Dalton Minimum values and then continue to increase in line with the strengthening radiative forcing. At the same time trends in *FW* storage become positive and are better constrained, i.e., the ensemble members' spread becomes smaller. This indicates a robust response to the change in forcing. Trends in sea ice storage, however, remain around zero until the end of the nineteenth century when they finally become negative in all ensemble members. This means that the increase in *FW* storage just after the Dalton

Minimum cannot be attributed to a redistribution of the freshwater from sea ice to the ocean. It rather seems that the synchronous increases of total $P-E$ and R after their forcing-induced minimum during the Dalton Minimum are responsible for the freshening ocean. This increase of total $P-E$ and R is consistent with the significant and robust increase of VQ and Q from the Dalton Minimum to Pre-industrial (Table 2).

This leads to the conclusion that the mean state of the Arctic freshwater balance during Initial Conditions, the Maunder Minimum, and the Dalton Minimum is fairly stable, the exception being small but significant differences in the freshwater reservoirs which seem to reflect the multi-decadal to centennial variations in the external forcing. During the sustained cold conditions of the Maunder Minimum a saltier ocean, more sea ice and less water vapor (compared to the onset of the Little Ice Age at 1500 AD) were the marked anomalies in the freshwater balance. During the Dalton Minimum a short-lived response of the atmospheric component of the freshwater cycle occurred. However, the small signal-to-noise ratio indicates the important role of the internal variability of the freshwater cycle.

3.3 Future projections

The changes in the freshwater budget projected for the Future Projections are substantial and very robust, as for every investigated budget term all four ensemble members show a significant difference in mean compared to our reference Present-Day. VQ is roughly 27% larger than during Present-Day, caused by the thermally induced increase of the moisture holding capacity. At the same time the volume transport remains largely unchanged, which is reflected also in the cyclone activity in the domain: Both the number and mean intensity of the cyclones stay constant in winter and even decrease slightly in spring, summer, and autumn for the Future Projections (not shown). This confirms that the strengthened atmospheric water import is due to the amount of water transported by cyclones rather than by an increase of their frequency or intensity. Cyclones are detected as minima in the 12-hourly 1,000 hPa geopotential height field and need to exceed a gradient of 20 gpm 1,000 km⁻¹ across a surrounding area of 1,000 km × 1,000 km (a detailed description of the cyclone detection and tracking method is given in Raible et al. 2007, 2010). The additional precipitable water in the domain is the reason for an increase of total P . As annual mean sea ice extent is reduced by 12% compared to Present-Day (not shown) the open ocean area grows and receives much more P directly from the atmosphere (+43%). Runoff from lower latitudes and $P_{Ind}-E_{Ind}$ increase as well, leading to a substantial increase in R to the

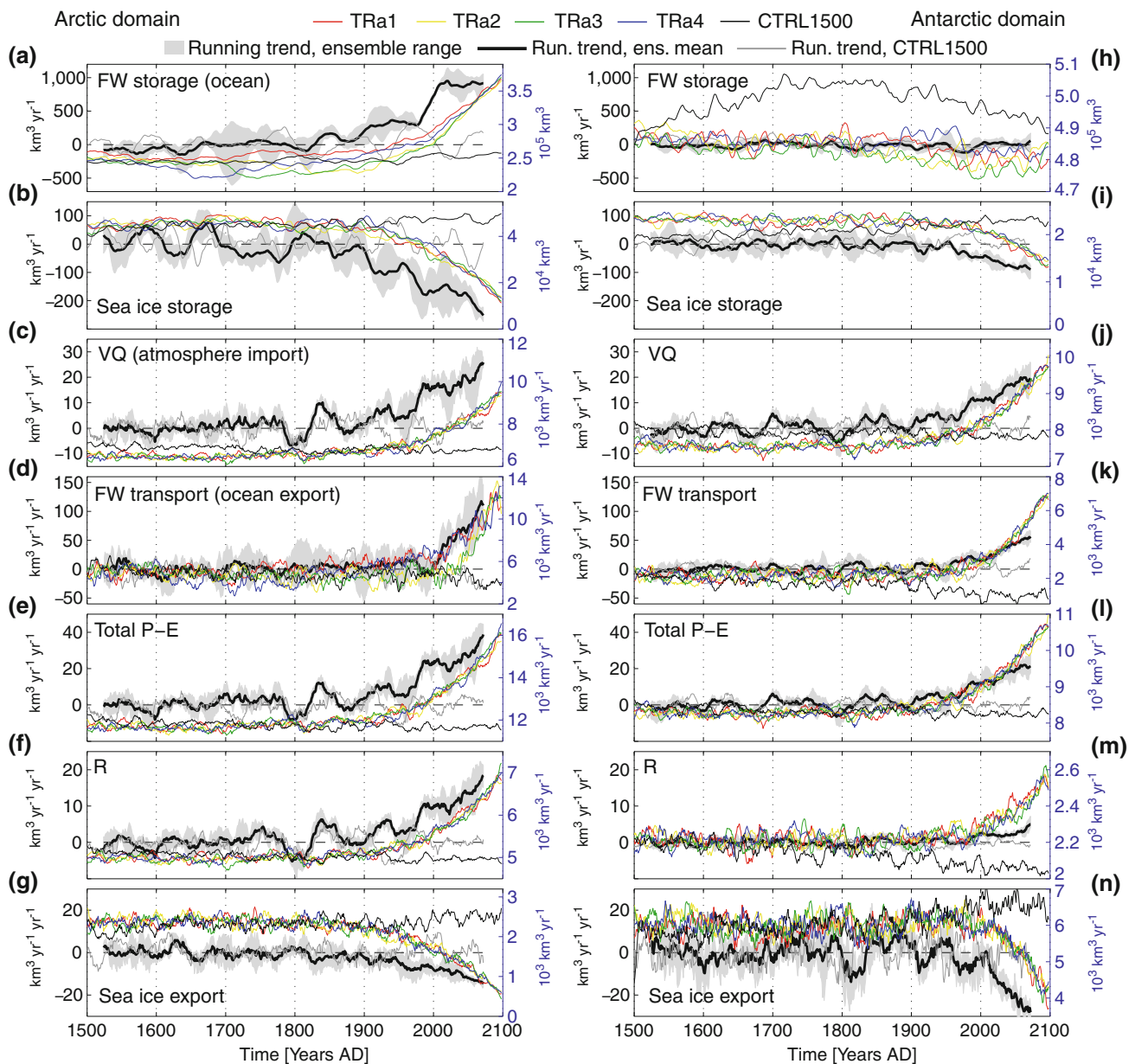


Fig. 8 Time series and trends of polar freshwater storage and transport terms. 50 Years running trends (ensemble range in gray shading, ensemble mean as thick black line, CTRL1500 as gray line; left black y-axis) and 5 years running means (transient simulations as colored lines, CTRL1500 as thin black line; right blue y-axis) of FW storage, sea ice storage, VQ, FW transport, total P–E, R, and sea ice

export for the Arctic (a–g) and Antarctic domain (h–n). Values are plotted at the middle-year of the 50 and 5 years window, respectively. A narrow shading of the running trend indicates a consistent behavior of the ensemble members, i.e., potentially externally forced variations. Opposed to that, a large spread of the shading indicates a period dominated by internal variability

ocean of roughly 26% (manifested in the positive anomalies close to the river’s discharge areas in Fig. 7a, bottom panel). Further, the annual mean melt-freeze ratio of sea ice rises from 1.05 during Present-Day to 1.15 during the Future Projections, representing an enhanced release of sea ice-stored freshwater to the ocean (due to the large sea ice volume at present-day no sea ice-free summer conditions are reached in these simulations). This leads to a spatial shift in the freshwater flux to the ocean surface, causing

strong local anomalies in the GIN Seas (Fig. 7a, bottom panel). Together with R, sea ice is the main driver of changes in the ocean freshwater budget.

Overall, the freshwater flux from $P_{ocn} - E_{ocn}$ and R to the Arctic domain’s ocean increases by 39% from Present-Day to the Future Projections. Consequently, the export of freshwater from the Arctic Ocean is strongly increased as well during the twenty-first century. Sea ice export, on the other hand, is decreased in all sectors and disappears

completely in the eastern Bering Sea and in the Labrador sector (Fig. 7). The latter causes the *FW* storage in the GIN Seas to decrease as less sea ice is transported there. This mechanism has been identified to counteract temperature-driven stratification and thereby maintaining deep-water formation in the GIN Seas (Holland et al. 2006b). The vast rest of the Arctic domain's ocean is freshening during the twenty-first century. The largest changes occur in the Beaufort Gyre, which strengthens and increases its freshwater storage in the future (Fig. 4). Correlation and trend analysis suggest that, due to its proximity to the Beaufort Gyre, the *FW* transport through the CAA is coupled directly to the growing *FW* storage in the Gyre (not shown). Together with increased surface freshwater forcing in the CAA (Fig. 7a, bottom panel) and a growing sea surface height gradient across the CAA (as described by Jahn et al. (2010) for interannual transport variability) this results in an increase of the *FW* transport in the Labrador sector over the twenty-first century. This increase is about three times stronger than the increase of *FW* transport in the Irminger Sea sector (Fig. 7). The freshwater import through the Bering Strait decreases in line with the weakening of the meridional pressure gradient across the Bering Strait due to the freshening Arctic Ocean (Arzel et al. 2008).

The findings for the mean changes from Present-Day to the Future Projections are generally in agreement with numerous model studies focusing on the Arctic Ocean only (Holland et al. 2006a, b; Koenigk et al. 2007; Arzel et al. 2008). In some respect, however, different models still perform differently. Koenigk et al. (2007) project the Arctic Ocean total freshwater export to stay fairly constant until the twenty-second century, i.e., the decrease in sea ice export is matched by the increase in the liquid export. We find, when considering either the Arctic Ocean only or the complete Arctic domain north of 60°N, that the ocean increases its total export of freshwater significantly already during the twenty-first century. Arzel et al. (2008) discovered a threshold behavior of the Fram Strait through-flow as a consequence of ocean-atmosphere heat exchange in an A1B simulation which was not reproduced in our simulations. Here, the Fram Strait volume flux stays constant. The increase in *FW* transport, which we find in the Fram Strait, is mainly due to fresher waters transported and not due to changes in the volume flux (not shown). The proposed mechanism of Arzel et al. (2008) requires a strong reduction of sea ice in the Barents Sea at the beginning of the twenty-first century and a freshening of the GIN Seas in the late twenty-first century. While the first of these features occurs to a lesser extent (not shown), the second is not simulated at all in the CCSM3 (see Fig. 7).

Regarding the transient behavior of the freshwater budget remarkable changes in the trends of *FW* storage and

sea ice storage are found in the second half of the twentieth century when these two terms accelerate their growth and decay rate by a factor of about two, respectively (Fig. 8). At the same time, the transport terms VQ , total $P-E$, and R show a strong increase to more positive trends as well. This indicates that a large part of the change in the Arctic freshwater cycle is evident well before the maximum warming in the simulations. This is in agreement with Arctic Ocean-only results from one high-resolution CCSM3 simulation using the A2 scenario (Holland et al. 2006b). There, solid and liquid freshwater transport as well as runoff show their largest changes in the period of 1975–2025 AD, in line with an ensemble using the A1B scenario (Holland et al. 2006b). The A1B scenario projects a GHGs concentration peak around 2050 AD. In our case, using the A2 scenario and the domain of 60–90°N, the same terms (*FW* transport, sea ice export, and R) have their largest trends at the end of the twenty-first instead of the twentieth century. A possible cause for this disagreement is the overestimation of end-twentieth century sea ice volume in our simulations. This delays polar amplification (Holland and Bitz 2003) and the peak in sea ice export and sea ice melt flux, which both occur later in the low-resolution CCSM3 ensemble. While we overestimate the absolute amount of sea ice in the Arctic Ocean, the evolution and amount of sea ice lost in the twenty-first century are similar to the high-resolution CCSM3 (Fig. 9b). A direct comparison of flux terms for the domain 60–90°N from low- and high-resolution CCSM3 simulations shows that the trends of $P-E$ over the ocean, R , sea ice melt flux, and *FW* transport are similar (Fig. 9c). However, the low-resolution CCSM3 simulation has a weaker *FW* transport resulting in a faster accumulation of *FW* during the twenty-first century. This strong *FW* storage increase is at the higher end in comparison to other models, but still falls within the standard deviation (Fig. 9a).

4 Freshwater balance of the Antarctic domain

4.1 Present-day climate

The Antarctic domain is characterized by a completely different geographic setting compared to the Arctic. 63% of the domain's area as well as the domain's lateral boundaries at 60°S are covered by ocean, which—together with a larger atmospheric mass transport (not shown)—results in more water vapor advected (VQ) to the Antarctic domain than to the Arctic domain (Fig. 6). Due to the dominant circumpolar circulation this import of water vapor is uniformly distributed along 60°S with a maximum in the sector north to the Ross Sea (Fig. 7). This corresponds well to observations (Tietäväinen and Vihma 2008). Total Q is

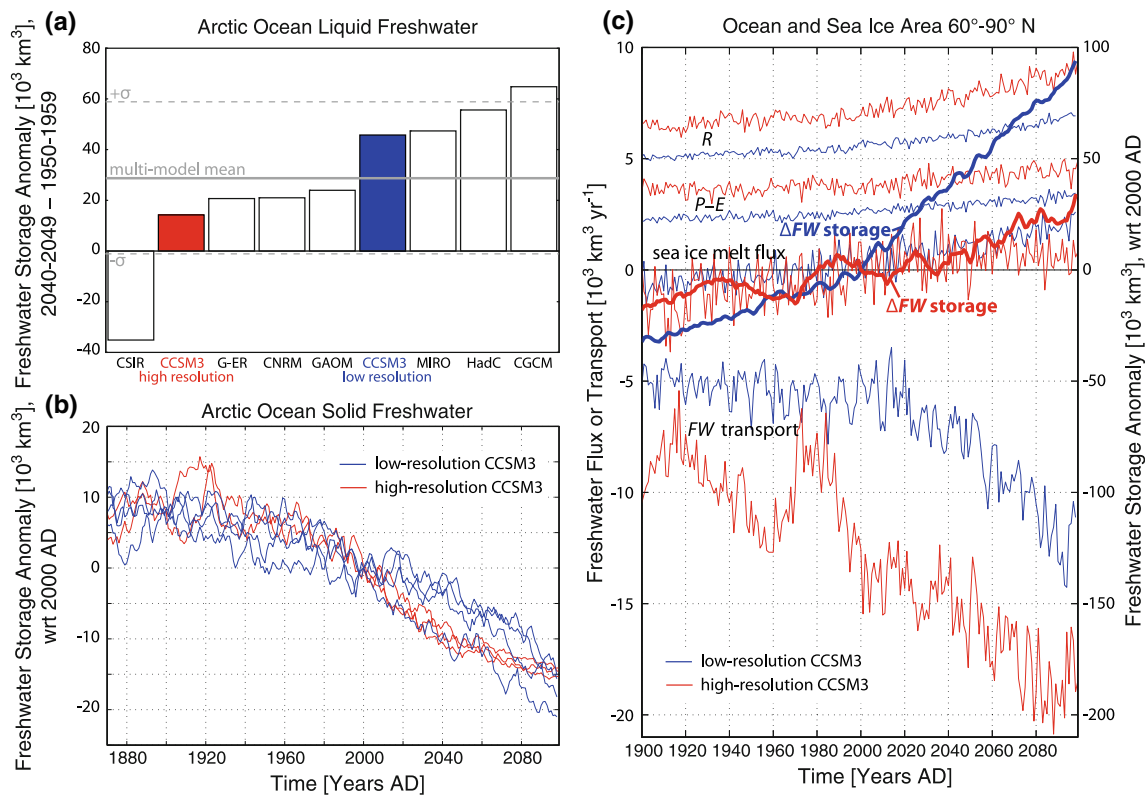


Fig. 9 **a** Change in Arctic Ocean freshwater storage of 2040–2049 AD relative to 1950–1959 AD from different models using a reference salinity of 34.8 g kg^{-1} . CCSM3 low-resolution corresponds to our ensemble mean. All other numbers are as in Fig. 11 from Holland et al. (2007) (M. Holland, pers. communication) and are based on the A1B scenario. Further details on these simulations in Holland et al. (2007). Note that our ensemble uses the A2 scenario, however, the forcing is very similar to the A1B scenario for the time

period 1950–2049 AD (IPCC 2007). **b** Arctic Ocean sea ice storage as anomaly to the year 2000 AD from simulations with the high-resolution CCSM3, applying the A2 scenario, and our ensemble. **c** Freshwater fluxes and transports to the ocean at 60–90°N (left axis) and the anomalous ocean freshwater storage (reference salinity 34.88 g kg^{-1}) from one high-resolution CCSM3 simulation and our ensemble mean (right axis)

smaller than over the Arctic domain owing to the lower temperatures, especially south of 70°S, i.e., over the Antarctic ice sheet (not shown).

For the larger part, P falls on the sea ice and ocean surface while the Antarctic ice sheet receives only about 19% of total P during the reference period Present-Day. Due to the lower temperatures the portion of P that is evaporated to the atmosphere is smaller than in the Arctic domain. P over the ice sheet falls mainly as snow (not shown), which means that R is made up solely by the melt flux from the terrestrial snow layers.

During Present-Day the sea ice freshwater balance is positive as illustrated by the sea ice melt-freeze ratio of 0.96 ($800 \text{ km}^3 \text{ year}^{-1}$). However, as sea ice is exported at a rate of about $6,100 \text{ km}^3 \text{ year}^{-1}$ (more than a factor three of the Arctic domain’s export rate during Present-Day) the sea ice volume shrinks nonetheless during Present-Day. In agreement with Schmitt et al. (2004), the vast majority of the sea ice export takes place north of the Weddell Sea (Fig. 7). As the FW transport in the Antarctic domain has

to be calculated from the residuals of the FW storage changes and the ocean surface fluxes, we cannot split it up into sectors. However, investigating a few years of sub-daily output the model has proven to be capable of simulating the Drake Passage effect (e.g., Talley 2008), i.e., the major freshwater export due to Ekman transport in the Drake Passage and the smaller return flow in the Atlantic sector.

4.2 Preindustrial changes

Looking at the preindustrial time periods Initial Conditions and the Maunder Minimum, the mean differences compared to Present-Day are generally less robust than in the Arctic domain. This could already be anticipated from the smaller preindustrial temperature anomalies in the Antarctic domain (Fig. 2). Nevertheless, we find significant reductions in VQ and Q during Initial Conditions and the Maunder Minimum (Fig. 6). Thereby the changes in VQ are uniformly distributed across the sectors, i.e., no large

changes in certain sectors dominate the total change in VQ (Fig. 7). This reduced VQ results in less total P and $P-E$, in turn influencing the FW transport, which is significantly smaller during the Maunder Minimum in three of the ensemble members. R and the export of sea ice remain unchanged. The melt and freeze rates of sea ice are significantly different compared to Present-Day, but not the ratio of the two. Therefore, sea ice production during Initial Conditions and the Maunder Minimum is only about $100 \text{ km}^3 \text{ year}^{-1}$ larger than during Present-Day. As a consequence the difference in sea ice volume between the preindustrial time periods and Present-Day is small, but significant in three ensemble members nevertheless (Fig. 6). When comparing with the first half of the twentieth century instead of Present-Day the difference quickly becomes insignificant. This confirms results by Sedláček and Mysak (2009), who found no significant long-term trend in simulated Southern Hemisphere sea ice volume between 1500 and about 1950 AD (see also our Fig. 8i). This means that the ocean and sea ice freshwater budget during Initial Conditions, the Maunder Minimum, and Present-Day are primarily controlled by the atmospheric input and stay approximately in balance. Note, however, that the unstable behavior of the FW storage in the CTRL1500 (Fig. 8h) points to a potential inaccuracy of the FW transport calculated from monthly means.

As in the Arctic domain, most variations within the preindustrial era in the Antarctic freshwater balance are not robust. In fact, only the reduction of the FW storage from Initial Conditions to the Maunder Minimum is significant in all four ensemble members (Table 2). At the same time, two members show a significant increase in sea ice storage. As no notable change in the total amount of freshwater in the domain is detectable, i.e., the fluxes at the boundary stay constant, this corresponds to a shift of freshwater from the ocean to the sea ice. However, the signal-to-noise ratio does not allow for an attribution to the external forcing. The same holds true for the comparison of Preindustrial with Initial Conditions, the Maunder Minimum, and the Dalton Minimum: no robust signal can be detected for any quantity of the budget as either significance is not reached or the ensemble members show significant, though opposed trends. This is not surprising as the Antarctic SAT during preindustrial times does not resemble the forcing variations such as the Maunder Minimum or the Dalton Minimum.

Similar to the high northern latitudes, the volcanic eruptions during the Dalton Minimum do not leave a significant imprint in the $P-E$ and VQ fields south of 60°S . This result is confirmed by the mean response of $P-E$ and VQ to the 21 largest eruptions from 1500–2000 AD in our simulations, as well as a case study of the atmospheric circulation response to Pinatubo (Robock

et al. 2007). The response is even weaker than in the high northern latitudes as the larger ocean area of the SH dampens the radiative perturbation from the erupted aerosols (Robock 2000) and as the stronger polar vortex of the SH is thought to be more resistant to perturbations (Stenchikov et al. 2002).

4.3 Future projections

For the Future Projections the changes are, similar to the Arctic domain, very robust as nearly all budget and flux terms in all ensemble members experience a significant shift in mean. The domain is fed by 20% more water vapor compared to Present-Day which mainly arises from increased moisture content (Liu and Curry 2010). The largest increase in VQ occurs in the Bellinghausen Sea (Fig. 7) where the frequency of occurrence of cyclones decreases, but on average cyclones carry more moisture into the domain (not shown, see also Lambert and Fyfe 2006; Lynch et al. 2006). As in the Arctic, the majority of this additional freshwater is precipitated onto the open ocean surface, which is enlarged due to the reduction of the sea ice area (-11% , not shown). The sea ice storage is reduced by 32%, indicating that sea ice is substantially thinned. This increases the freshwater flux to the ocean surface in large regions of the Southern Ocean south of 55°S (Fig. 7b, bottom panel). While sea ice export weakens in nearly all longitudinal sectors (Fig. 7), the export by FW transport strengthens. The latter dominates these changes as export substantially exceeds the import during the twenty-first century.

5 Summary and conclusion

We use an ensemble of four transient simulations with the low-resolution version of the CCSM3, spanning the time period from 1500 to 2100 AD, to investigate past and future changes of the polar freshwater balance. The simulations produce a realistic general NH temperature evolution over the past five centuries with an overestimated warming in the twentieth century due to missing aerosols (Hofer et al. 2011). Temperatures on the poles, however, are rather underestimated. The simulated present-day freshwater cycle of the Arctic Ocean agrees reasonably well with observations (Serreze et al. 2006), except that freshwater stored in sea ice and ocean is overestimated significantly.

We show that many of the transport and storage components in the present-day polar freshwater cycle are significantly different from preindustrial states and in particular from the projected future state. While this conclusion is valid for both polar domains the relative

magnitude of the differences is larger in the Arctic where temperature anomalies in the past and future are larger as well.

Regarding the Arctic, the simulated freshwater cycle appears to be closely coupled to temperature on decadal time scales. We showed this for the twentieth and twenty-first century in consistency with other model studies (Gosse and Holland 2005; Holland et al. 2007) as well as observational records (White et al. 2007). This relationship was found to hold beyond the temporal scope of the studies mentioned before as during the cold phase of the Little Ice Age simulated freshwater transports are smaller than during present-day and the domain contains less freshwater in total. As temperature rises during the twentieth and twenty-first century more water passes through the hydrological cycle and the reservoir of *FW* grows at the expense of the reservoir of sea ice and due to increased $P-E$ and R . Synchronously, the *FW* transport increases and represents a strengthening freshwater forcing to the North Atlantic. These features are consistent among most coupled GCMs (Holland et al. 2007), however, the magnitude of change depends on the model and its resolution. This is particularly evident for the reservoirs of sea ice and *FW*. Compared to the high-resolution CCSM3 the low-resolution has a weaker ocean heat transport into the Arctic and a weaker *FW* transport out of the Arctic. Resulting from that, sea ice is overestimated in this study, leading in turn to a lagged peak of freshwater release in the future. At the same time, the weak *FW* transport yields a reservoir of *FW* that grows faster than in the high-resolution CCSM3. Based on this, the magnitude of preindustrial changes might be model-dependent as well, which needs to be considered when interpreting these results.

Within the preindustrial era of 1500–1870 AD the Arctic domain's total amount of freshwater is largely controlled by VQ while for the present and future the changes in *FW* transport and sea ice export contribute crucially as well.

Sedláček and Mysak (2009) showed that during preindustrial times wind-stress plays an equally important role as direct radiative effects regarding changes in sea ice volume and ocean properties in the Arctic. At the same time, the sea ice volume was found to be basically insensitive to changes in radiative forcing as they occurred during the Maunder Minimum and the Dalton Minimum. We are unable to depict this hypothesis as precisely as the sensitivity study of Sedláček and Mysak (2009). At least we see a weak but significant response of sea ice storage and *FW* storage to changes in the external forcing occurring from 1500 AD to the Maunder Minimum. The Dalton Minimum, on the other hand, leaves no imprint on the sea ice and ocean freshwater storage, as its duration is too short to significantly affect these slow-reacting reservoirs. The atmospheric quantities of total $P-E$, VQ , and Q , on the

other hand, display a clear dip during the Dalton Minimum, forced primarily by the sun.

As our domain 60–90°N includes Greenland, in contrast to many other studies focusing on the Arctic Ocean only, we need to account for potential melt fluxes from the Greenland ice sheet when assessing the present-day and future state of this domain's freshwater balance. The processes of a melting or disintegrating ice sheet are not simulated by the land component of the CCSM3 due to the absence of a dynamic ice sheet model. However, recent estimates of both present-day ($267 \pm 38 \text{ km}^3 \text{ year}^{-1}$; Rignot et al. 2008) and future (year 2100 AD, $220 \text{ km}^3 \text{ year}^{-1}$, Ren et al. 2011; $>400 \text{ km}^3 \text{ year}^{-1}$, Graverson et al. 2011) Greenland mass balance are a magnitude smaller than the changes projected for other freshwater fluxes such as P , R , or the melting of sea ice. The projected acceleration of the Greenland mass loss by about $100\text{--}200 \text{ km}^3 \text{ year}^{-1}$ over the twenty-first century even lies within the ensemble uncertainty for, e.g., changes in R or sea ice melting. Therefore, the absence of an ice sheet model does not render the Arctic freshwater balance of the CCSM3 unrealistic. Similar conclusions can be drawn for the Antarctic domain, where recent literature suggests the twenty-first century contribution of freshwater from the ice sheet ($<500 \text{ km}^3 \text{ year}^{-1}$, Pfeffer et al. 2008; Katsman et al. 2011) to be substantially smaller than changes in other components of the ocean's surface freshwater balance, e.g., $P-E$ ($+1,400 \text{ km}^3 \text{ year}^{-1}$). However, the estimates and projections from current literature for the Antarctic mass balance are far less robust than the ones for Greenland. Taking into account all possible scenarios in Pfeffer et al. (2008) and Katsman et al. (2011) it remains uncertain, whether the Antarctic ice sheet will retain a close-to-zero mass balance or become a significant source of freshwater within the twenty-first century.

The Antarctic domain's response to changes in external forcing is expected to be dampened compared to the Arctic. This is due to the more zonal circumpolar current in both atmosphere and ocean, hampering the heat exchange with lower latitudes, as well as the larger ocean area, acting to reduce amplitudes in surface warming due to changes in the radiative balance (IPCC 2007). Additionally, the ice and snow albedo feedback is smaller in the Antarctic domain (Masson-Delmotte et al. 2006). This was confirmed in our study as anomalies in the freshwater cycle are smaller than in the Arctic.

During the preindustrial period no significant and robust changes in the individual terms of the Antarctic freshwater balance could be detected from our ensemble, suggesting that minima in external forcing (Maunder Minimum, Dalton Minimum) do not leave an imprint on the SH high latitudes' water cycle. As *FW* transport and sea ice export

do not change much during the first 450 years, the atmospheric import VQ is the controlling mechanism regarding the domain's total freshwater content. The future projections then show a substantial acceleration of the hydrological cycle, affecting all fluxes, with a linear dependence on the SAT projections. Thereby, the strongly increasing FW transport strengthens the Antarctic domain as a freshwater source to the lower latitude oceans. Liu and Curry (2010) stress the potentially too weak response of the twentieth century Southern Ocean climate to anthropogenic forcing in models due to an overestimated sea surface temperature internal variability. Taking into account this and a possible lack of decadal SAT variability in the southern high latitudes of the model, the simulated amplitudes in the budget and transport terms of the Antarctic domain have to be interpreted with caution as they might have been larger during preindustrial times than simulated in this study. Therefore, other millennial simulations with new and higher resolved models are in need, which – together with proxies – will add to the picture of past variations of the polar freshwater reservoirs.

Acknowledgments We gratefully acknowledge Andreas Born for valuable discussion, as well as two anonymous reviewers for constructive comments. We are grateful to the ECMWF, the NASA GISS, the NOAA ESRL, the ESG, Igor Polyakov, and Marika Holland for providing access to data and to the NCAR for providing the code of the CCSM3 model. This study is supported by the National Centre of Competence in Research (NCCR) Climate funded by the Swiss National Science Foundation, and the European Commission Past4Future project. The simulations were performed on an IBM Power 4, a CRAY XT3, and a CRAY XT5 at the Swiss National Supercomputing Centre (CSCS) in Manno.

Open Access This article is distributed under the terms of the Creative Commons Attribution Noncommercial License which permits any noncommercial use, distribution, and reproduction in any medium, provided the original author(s) and source are credited.

References

- ACIA (2005) Impacts of a warming Arctic. Arctic climate impact assessment. Cambridge University Press, Cambridge
- Allen MR, Ingram WJ (2002) Constraints on future changes in climate and the hydrological cycle. *Nature* 419:224–232
- Arzel O, Fichet T, Goosse H, Dufresne JL (2008) Causes and impacts of changes in the Arctic freshwater budget during the twentieth and twenty-first centuries in an AOGCM. *Clim Dyn* 30:37–58
- Bekryaev RV, Polyakov IV, Alexeev VA (2010) Role of polar amplification in long-term surface air temperature variations and modern Arctic warming. *J Clim* 23:3888–3906
- Bryan FO, Danabasoglu G, Nakashiki N, Yoshida Y, Kim DH, Tsutsui J, Doney SC (2006) Response of the North Atlantic thermohaline circulation and ventilation to increasing carbon dioxide in CCSM3. *J Clim* 19:2382–2397
- Collins WD et al (2006) The community climate system model: CCSM3. *J Clim* 19:2122–2143
- Compo G et al (2010) The twentieth century reanalysis project. *Q J R Meteorol Soc* 137:1–28
- Goosse H, Holland MM (2005) Mechanisms of decadal Arctic climate variability in the community climate system model, version 2 (CCSM2). *J Clim* 18:3552–3570
- Graversen RG, Drijfhout S, Hazeleger W, van de Wal R, Bintanja R, Helsen M (2011) Greenland's contribution to global sea-level rise by the end of the 21st century. *Clim Dyn*. doi:10.1007/s00382-010-0918-8
- Hack J, Caron J, Yeager SG, Oleson KW, Holland MM, Truesdale JE, Rasch PJ (2005) Simulation of the global hydrological cycle in the CCSM community atmosphere model version 3 (CAM3): mean features. *J Clim* 19:2199–2221
- Hansen J, Ruedy R, Sato M, Lo K (2010) Global surface temperature change. *Rev Geophys* 48:RG4004. doi:10.1029/2010RG000345
- Held IM, Soden BJ (2006) Robust responses of the hydrological cycle to global warming. *J Clim* 19:5686–5699
- Hofer D, Raible CC, Stocker TF (2011) Variations of the Atlantic meridional overturning circulation in control and transient simulations of the last millennium. *Clim Past* 7:133–150
- Holland MM, Bitz CM (2003) Polar amplification of climate change in coupled models. *Clim Dyn* 21:221–232
- Holland MM, Bitz CM, Hunke EC, Lipscomb WH, Schramm JL (2006) Influence of the sea ice thickness distribution on polar climate in CCSM3. *J Clim* 19:2398–2414
- Holland MM, Finnis J, Barrett AP, Serreze MC (2007) Projected changes in Arctic Ocean freshwater budgets. *J Geophys Res* 112:G04S55
- Holland MM, Finnis J, Serreze MC (2006) Simulated Arctic Ocean freshwater budgets in the twentieth and twenty-first centuries. *J Clim* 19:6221–6242
- Huntington TG (2005) Evidence for intensification of the global water cycle: review and synthesis. *J Hydrol* 319:83–95
- IPCC (2001) Climate change 2001, the scientific basis. Intergovernmental panel on climate change. Cambridge University Press, Cambridge
- IPCC (2007) Climate change 2007, the science of climate change. Intergovernmental panel on climate change. Cambridge University Press, Cambridge
- IPCC SRES (2000) Special report on emissions scenarios. Intergovernmental panel on climate change, Cambridge University Press, Cambridge
- Jahn A, Tremblay B, Mysak LA, Newton R (2010) Effect of the large-scale atmospheric circulation on the variability of the Arctic Ocean freshwater export. *Clim Dyn* 34:201–222
- Katsman CA et al (2011) Exploring high-end scenarios for local sea level rise to develop flood protection strategies for a low-lying delta—the Netherlands as an example. *Clim Change*. doi:10.1007/s10584-011-0037-5, published online
- Khon VC, Park W, Latif M, Mokhov II, Schneider B (2010) Response of the hydrological cycle to orbital and greenhouse gas forcing. *Geophys Res Lett* 37:L19 705
- Kiehl JT, Shields CA, Hack JJ, Collins WD (2006) The climate sensitivity of the community climate system model version 3 (CCSM3). *J Clim* 19:2584–2596
- Koenigk T, Mikolajewicz U, Haak H, Jungclaus J (2007) Arctic freshwater export in the 20th and 21st centuries. *J Geophys Res* 112:G04S41
- Lambert SJ, Fyfe JC (2006) Changes in winter cyclone frequencies and strengths simulated in enhanced greenhouse warming experiments: results from the models participating in the IPCC diagnostic exercise. *Clim Dyn* 26:713–728
- Liu J, Curry R (2010) Accelerated warming of the Southern Ocean and its impacts on the hydrological cycle and sea ice. *Proc Natl Acad Sci USA* 107:14987–14992

- Lynch A, Uotila P, Cassano JJ (2006) Changes in synoptic weather patterns in the polar regions in the twentieth and twenty-first centuries, part 2: Antarctic. *Int J Climatol* 26:1181–1199
- Mann EM et al (2009) Global signatures and dynamical origins of the little ice age and medieval climate anomaly. *Science* 326:1256–1260
- Masson-Delmotte V et al (2006) Past and future polar amplification of climate change: climate model intercomparisons and ice-core constraints. *Clim Dyn* 26(5):513–529. doi:[10.1007/s00382-005-0081-9](https://doi.org/10.1007/s00382-005-0081-9)
- Pardaens AK, Banks HT, Gregory JM, Rowntree PR (2003) Freshwater transports in HadCM3. *Clim Dyn* 21:177–195
- Peterson BJ, Holmes RM, McClelland JW, Vörösmarty CJ, Lammers RB, Shiklomanov AI, Shiklomanov IA, Rahmstorf S (2002) Increasing river discharge to the Arctic Ocean. *Science* 298:2171–2173
- Peterson BJ, McClelland JW, Curry R, Holmes RM, Walsh JE, Aagaard K (2006) Trajectory shifts in the Arctic and Subarctic freshwater cycle. *Science* 313:1061–1066
- Pfeffer WT, Harper JT, O’Neil S (2008) Kinematic constraints on glacier contributions to 21st-century sea-level rise. *Science* 321:1340–1343.
- Raible CC, Baruch Z, Saaroni H, Wild M (2010) Winter synoptic-scale variability over the Mediterranean Basin under future climate conditions as simulated by the ECHAM5. *Clim Dyn* 35:473–488
- Raible CC, Yoshimori M, Stocker TF, Renold M, Casty C (2007) Extreme midlatitude cyclones and their implications for precipitation and wind speed extremes in simulations of the Maunder Minimum versus present day conditions. *Clim Dyn* 28:409–423
- Rawlins MA et al (2010) Analysis of the Arctic system for freshwater cycle intensification: observations and expectations. *J Clim* 23:5715–5737
- Rayner N, Parker D, Horton E, Folland C, Alexander L, Rowell D, Kent E, Kaplan A (2003) Global analyses of sea surface temperature, sea ice, and night marine air temperature since the late nineteenth century. *J Geophys Res* 108:ACL2–1–29
- Ren D, Fu R, Leslie LM, Chen J, Wilson CR, Karoly DJ (2011) The Greenland ice sheet response to transient climate change. *J Clim* 24:3469–3483
- Rignot E, Box JE, Burgess E, Hanna E (2008) Mass balance of the Greenland ice sheet from 1958 to 2007. *Geophys Res Lett* 35:L20502
- Robock A (2000) Volcanic eruption and climate. *Rev Geophys* 38:191–219
- Robock A, Adams T, Moore M, Oman L, Stenchikov G (2007) Southern Hemisphere atmospheric circulation effects of the 1991 Mount Pinatubo eruption. *Geophys Res Lett* 34. doi:[10.1029/2007GL031403](https://doi.org/10.1029/2007GL031403)
- Schmitt C, Kottmeier C, Wassermann S, Drinkwater M (2004) Atlas of Antarctic Sea Ice Drift. Institute for Meteorology and Climate Research, University of Karlsruhe, Karlsruhe
- Schneider DP, Ammann CM, Otto-Bliesner BL, Kaufman DS (2009) Climate response to large, high-latitude and low-latitude volcanic eruptions in the community climate system model. *J Geophys Res* 114. doi:[10.1029/2008JD011222](https://doi.org/10.1029/2008JD011222)
- Seager R, Naik N, Vecchi GA (2010) Thermodynamic and dynamic mechanisms for large-scale changes in the hydrological cycle in response to global warming. *J Clim* 23:4651–4668
- Sedláček J, Mysak LA (2009) Sensitivity of sea ice to wind-stress and radiative forcing since 1500: a model study of the little ice age and beyond. *Clim Dyn* 32:817–831
- Serreze MC et al (2006) The large-scale freshwater cycle of the Arctic. *J Geophys Res* 111, 2005JC003424
- Sorteberg A, Walsh JE (2008) Seasonal cyclone variability at 70°N and its impact on moisture transport into the Arctic. *Tellus* 60:570–586
- Steele M, Morley R, Ermold W (2001) A global ocean hydrography with a high-quality Arctic Ocean. *J Clim* 14:2079–2087
- Stenchikov GI, Hamilton K, Stouffer RJ, Robock A, Ramaswamy V, Santer B, Graf HF, (2006) Arctic Oscillation response to volcanic eruptions in the IPCC AR4 climate models. *J Geophys Res* 111. doi:[10.1029/2005JD006286](https://doi.org/10.1029/2005JD006286)
- Stenchikov GL, Robock A, Ramaswamy V, Schwarzkopf M, Hamilton K, Ramachandran S, Oman L, (2002) Southern Hemisphere annular mode response to the 1991 Mount Pinatubo volcanic eruption. *Eos Trans AGU* 83, 13837–13858. Fall Meet. Suppl., Abstract A22D-09
- Stocker TF, Raible CC (2005) Water cycle shifts gear. *Nature* 434:830–832
- Syed TH, Famiglietti JS, Chambers DP, Willis JK, Hilburn K (2010) Satellite-based global-ocean mass balance estimates of interannual variability and emerging trends in continental freshwater discharge. *Proc US Natl Acad Sci* 107:17 916–17 921. doi:[10.1073/pnas.1003292107](https://doi.org/10.1073/pnas.1003292107)
- Talley L (2008) Freshwater transport estimates and the global overturning circulation: Shallow, deep and throughflow components. *Prog Oceanogr* 78:257–303
- Thompson DWJ, Solomon S (2002) Interpretation of recent Southern Hemisphere climate change. *Science* 296:895–899
- Tietäväinen H, Vihma T (2008) Atmospheric moisture budgets over Antarctica and the Southern Ocean based on the ERA-40 reanalysis. *Int J Climatol* 28:1977–1995
- Walsh JE (2009) A comparison of Arctic and Antarctic climate change, present and future. *Antarct Sci* 21:179–188
- White D et al (2007) The Arctic freshwater system: changes and impacts. *J Geophys Res* 112:G04S54
- Williams PD, Guilyardi E, Sutton R, Gregory J, Madec G (2007) A new feedback on climate change from the hydrological cycle. *Geophys Res Lett* 34. doi:[10.1029/2007GL029275](https://doi.org/10.1029/2007GL029275)
- Wu P, Wood R, Stott P (2005) Human influence on increasing Arctic river discharge. *Geophys Res Lett* 32:2004GL021 570
- Yeager SG, Shields CA, Large WG, Hack JJ (2006) The low-resolution CCSM3. *J Clim* 19:2545–2566
- Yoshimori M, Raible CC, Stocker TF, Renold M (2010) Simulated decadal oscillations of the Atlantic meridional overturning circulation in a cold climate state. *Clim Dyn* 34:101–121. doi:[10.1007/s00382-009-0540-9](https://doi.org/10.1007/s00382-009-0540-9)